



Ozone and fine particle in the western Yangtze River Delta: an overview of 1 yr data at the SORPES station

A. J. Ding¹, C. B. Fu¹, X. Q. Yang¹, J. N. Sun¹, L. F. Zheng¹, Y. N. Xie¹, E. Herrmann^{1,2}, W. Nie¹, T. Petäjä², V.-M. Kerminen², and M. Kulmala²

¹Institute for Climate and Global Change Research & School of Atmospheric Sciences, Nanjing University, Nanjing, 210093, China

²Department of Physics, University of Helsinki, 00014 Helsinki, Finland

Correspondence to: A. J. Ding (dingaj@nju.edu.cn)

Received: 8 January 2013 – Published in Atmos. Chem. Phys. Discuss.: 28 January 2013

Revised: 9 April 2013 – Accepted: 13 May 2013 – Published: 14 June 2013

Abstract. This work presents an overview of 1 yr measurements of ozone (O_3) and fine particulate matter ($PM_{2.5}$) and related trace gases at a recently developed regional background site, the Station for Observing Regional Processes of the Earth System (SORPES), in the western part of the Yangtze River Delta (YRD) in eastern China. Ozone and $PM_{2.5}$ showed strong seasonal cycles but with contrast patterns: O_3 reached a maximum in warm seasons but $PM_{2.5}$ in cold seasons. Correlation analysis suggests a VOC-sensitive regime for O_3 chemistry and a formation of secondary aerosols under conditions of high O_3 in summer. Compared with the National Ambient Air Quality Standards in China, our measurements report 15 days of O_3 exceedance and 148 days of $PM_{2.5}$ exceedance during the 1 yr period, suggesting a severe air pollution situation in this region. Case studies for typical O_3 and $PM_{2.5}$ episodes demonstrated that these episodes were generally associated with an air mass transport pathway over the mid-YRD, i.e., along the Nanjing–Shanghai axis with its city clusters, and showed that synoptic weather played an important role in air pollution, especially for O_3 . Agricultural burning activities caused high $PM_{2.5}$ and O_3 pollution during harvest seasons, especially in June. A calculation of potential source contributions based on Lagrangian dispersion simulations suggests that emissions from the YRD contributed to over 70 % of the O_3 precursor CO, with a majority from the mid-YRD. North-YRD and the North China Plain are the main contributors to $PM_{2.5}$ pollution in this region. This work shows an important environmental impact from industrialization and urbanization in the YRD region, and suggests an urgent need for improving

air quality in these areas through collaborative control measures among different administrative regions.

1 Introduction

Ozone (O_3) and fine particulate matter ($PM_{2.5}$) are two of the most important components in the tropospheric atmosphere because of their effects on human health, biosphere and climate (e.g., Chameides et al., 1999a, b; Jerrett et al., 2009; Allen et al., 2012). Because of complex sources and chemical reactions, and a relatively long atmospheric lifetime in the atmosphere that favors regional/long-range transport, both pollutants are of great concern for regional air quality but are very difficult to control (Cooper et al., 2005; Zhang et al., 2008; van Donkelaar et al., 2010).

Due to huge consumption of fossil fuels in the past decades (Richter et al., 2005), many regions in China have been experiencing heavy and even increasing O_3 and $PM_{2.5}$ pollution, especially in the developed coastal regions, such as the Beijing–Tianjin area, Pearl River Delta (PRD) and Yangtze River Delta (YRD) (Ding et al., 2008; Xu et al., 2008; Wang et al., 2009; Tie and Cao, 2009). In the latest decades, a large number of studies were performed to address their spatiotemporal distributions and to understand their causes in those developed regions. A relatively long history of research and hence a good understanding have been gained in the Beijing–Tianjin and the PRD regions (e.g., Zhang et al., 2003; Wang et al., 2003, 2006, 2009, 2010; Lin et al., 2008), while in the YRD region, in which only few measurement studies have

been conducted, large knowledge gaps still exist in the understanding of the characteristics and main sources of O₃ and PM_{2.5}.

The YRD region is located in the eastern part of the Yangtze Plain adjacent to the most polluted North China Plain (Fig. 1b). It includes the mega-city Shanghai and the well-industrialized and urbanized areas of the southern part of Jiangsu Province and the northern part of Zhejiang Province, with over ten mega/large cities, such as Hangzhou, Suzhou, Wuxi and Changzhou lying along the mid-YRD, i.e., the Shanghai–Nanjing axis (see Fig. 1c). Consisting of only 2 percent of the land area, this region produces over 20 percent of China's Gross Domestic Product (GDP), making it the most densely populated region in the country and one of its emission hotspots. Furthermore, this area and the surrounding Yangtze Plain also form one of the most important agricultural bases in China with wheat and rice planted alternatively in cold and warm seasons. Previous studies suggested that both O₃ and aerosols could affect the crop growth in this region (e.g., Feng et al., 2003; Chameidies, 1999a, b), and also suggest that agricultural activities, such as fertilization and intensive straw burning activities, could significantly influence regional air quality in this region (e.g., Ye et al., 2011, Wang et al., 2004, 2009; Ding et al., 2013b). In addition, the YRD is located in a typical monsoon region, with warm and humid conditions in summer and cold and dry weather in winter. The complex monsoon and synoptic weather may play an important role in air pollution transport and formation in this region. Therefore, this is a region of great interest to study the complex interactions between human activities, biosphere and the atmosphere.

The earliest measurement study of O₃ in the YRD region started in the 1990s at the Lin'an site, a regional station located in the southeast YRD (Luo et al., 2000; Wang et al., 2001). Studies at this site provided the first picture of the seasonal behaviors of O₃ and its precursors in the southeast YRD (Wang et al., 2001, 2004; Xu et al., 2008). Besides Lin'an, there were only very limited studies of O₃ made in urban areas in some YRD cities (e.g., Tu et al., 2007; Geng et al., 2008; Ran et al., 2012). PM_{2.5} measurements in this region have been performed only in recent years (e.g., Fu et al., 2008; Zhou et al., 2009; Li et al., 2011; Huang et al., 2012; Zhang et al., 2013). However, most of these studies were done close to Shanghai, i.e., the eastern YRD, and mainly cover short periods. For the more inland western YRD area, which is generally downwind from the entire YRD under prevailing winds between northeast and southeast, only very few studies of O₃ and PM_{2.5} were conducted, and these only at urban sites (e.g., Wang et al., 2002; Yang et al., 2005; Tu et al., 2007). Therefore, there is a significant lack of knowledge on the regional characteristics of these pollutants, which is inherently important for the assessment of the regional impacts of the YRD emissions on atmospheric composition and also for the policy making of air pollution measures in west YRD cities like Nanjing.

To fill the knowledge gap, continuous online measurements of trace gases, aerosols and other relevant parameters were carried out at a background site SORPES (Station for Observing Regional Processes of the Earth System), an integrated measurement platform for the study of atmospheric environment and climate change. This work presents the first results of 1 yr measurements of O₃ and PM_{2.5} and related trace gases at the site during August 2011–July 2012, and gives a synthetic analysis about their characteristics and sources by using Lagrangian dispersion modeling. We give detailed descriptions about the measurement site and instruments and an introduction of general meteorological conditions in Sect. 2, and present main results, including overall temporal variation, correlation analysis and case studies in Sect. 3. A summary is given in Sect. 4.

2 Description of experiment and meteorological conditions

2.1 Brief introduction to the SORPES site

The Station for Observing Regional Processes of the Earth system is a research and experiment platform developed by the Institute for Climate and Global Change Research (ICGCR) at Nanjing University (NJU) in collaboration with the University of Helsinki. The overall objective of this platform is to characterize the temporal variation of key parameters related to climate change and to understand the interactions of different regional processes of the Earth system in eastern China, a region strongly influenced by monsoon weather and by intensive human activities. With a joint effort between NJU and the University of Helsinki, SORPES is in the process of being developed into a SMEAR (Station for Measuring Ecosystem–Atmosphere Relations) type measurement station (Hari et al., 2009), but focuses more on the impact of human activities on the climate and on the environment system in the rapidly urbanized and industrialized YRD region. Considering the geography, climate, and the environment characteristics in eastern China, measurements at the SORPES sites focus on four major processes: land surface processes, air pollution–climate interaction, ecosystem–atmosphere interaction, and hydrology and water cycle. The entire platform will be developed into an integrated observation network with a “flagship” central site, a few outlying “satellite” sites and mobile platforms in the vicinity.

At the current stage, the efforts mainly focus on the development of the flagship central site, which is located on the Xianlin Campus of NJU in the suburban area northeast of Nanjing (118° 57' 10" E, 32° 07' 14" N), about 20 km from the downtown area (Fig. 1a). Since the prevailing winds in this region are from northeast and southeast in the cold and warm seasons, respectively, the Xianlin site is generally upwind from downtown Nanjing and can be considered as a regional background station for atmospheric chemistry studies.

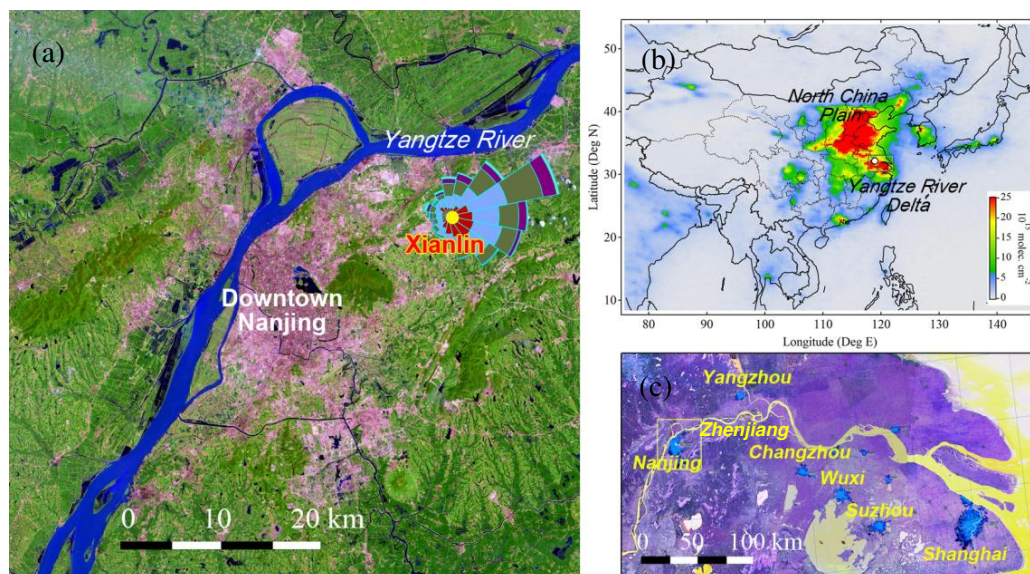


Fig. 1. (a) A map showing the location of the SORPES Xianlin site. (b) Averaged GOME2 tropospheric NO_2 columns for the period of August 2011–July 2012. (c) A map showing cities in the Yangtze River Delta. The GOME2 data were accessed from Tropospheric Emission Monitoring Internet Service of KNMI (Koninklijk Nederlands Meteorologisch Instituut or Royal Netherlands Meteorological Institute) (www.temis.nl).

As Nanjing is located in the northwest of the YRD region (Fig. 1c), the site is also generally downwind of the most developed mid-YRD regions including the megacity Shanghai and the Suzhou–Wuxi–Changzhou city cluster. Therefore, the measurements at the station can help address impacts from these areas of highly intensive human activity in a regional air quality perspective.

Measurements of trace gases, aerosols, and relevant meteorological parameters began in the summer of 2011. Most of the instruments are housed on the top floor of a laboratory building, which sits on the top of a hill about 40 m above the ground level. Trace gases like O_3 , carbon monoxide (CO), sulfur dioxide (SO_2), nitric oxide (NO), total reactive nitrogen (NO_y) and $\text{PM}_{2.5}$ mass were routinely measured. O_3 , SO_2 , NO, NO_y and CO trace gases were measured with a resolution of 1 min using online analyzers (Thermo Instruments, TEI 49i, 43i, 42i, 42iY and 48i, respectively). Ambient air was drawn from the 1.4 m above the rooftop to the laboratory building through a manifold connected to O_3 , SO_2 , NO and CO analyzers with PFA Teflon tubes (inside diameter: $\frac{1}{4}$ inch). A separate sample line with a MoO converter was used for NO_y analyzer. The length of sample lines for these trace gases are in a range of 6.5–7.3 m. $\text{PM}_{2.5}$ mass concentrations were measured using a mass analyzer (Thermo SHARP-5030), which has been used in many other studies and found to perform well for long-term runs (e.g., Petäjä et al., 2013). Since aerosols are quite hygroscopic in China (e.g., Eichler et al., 2008; Liu et al., 2011). The SHARP-5030 aerosol mass analyzer was operated un-

der dry conditions, with a 1 m long DHS heater settled up to keep the RH of samples no larger than 35 %. Besides $\text{PM}_{2.5}$ mass, aerosol size distribution measurements were also available since November 2011 by using an Air Ion Spectrometer (AIS) and differential mobility particle sizer (DMPS), and those data were reported in a companion paper (Herrmann et al., 2013).

The instrument precision was ± 2 ppbv for O_3 and ± 3 %, ± 1 %, ± 10 % and ± 4 % for SO_2 , CO, NO and NO_y , respectively. For SHARP $\text{PM}_{2.5}$, the precision was $\pm 2 \mu\text{g m}^{-3}$ for a concentration below $80 \mu\text{g m}^{-3}$ and $\pm 5 \mu\text{g m}^{-3}$ for a concentration over $80 \mu\text{g m}^{-3}$. All trace gas analyzers were weekly span calibrated and daily zero checked, and multi-point calibration was made once a month. N-propyl nitrate (NPN) was used to calibrate the NO_y converter, and the converter efficiency was higher than 95 % during the 1 yr measurement period. It should be pointed out that during the 1 yr period of this study, at the foot of the hill upon which the SORPES site is located there were some construction works, which may have occasionally influenced the site. However, because these activities were not upwind and emissions from these activities (such as windblown soil dust) were mainly in coarse mode, the fine particle and trace gases concentrations were rarely influenced by these activities. For the 1 yr period (August 2011–July 2012), these instruments performed well and data coverage of most of the species were higher than 95 %.

Meteorological measurements have been available at the site with Automatic Weather Station (CAMPBEL co., AG1000) since December 2011 but there was a data gap in

early 2012. However, in this study we used meteorological parameters, such as pressure, air temperature, relative humidity and precipitation, recorded at a site about 2.5 km west of the SORPES station run by Nanjing Meteorological Bureau. Available concurrent measurements at the two sites suggest a very good correlation for most of these parameters.

2.2 Meteorological conditions and transport features

Monthly averaged general meteorological parameters at Nanjing are shown in Table 1. They suggest that the region had a contrasting air temperature in winter and summer, with monthly means from about 3 °C in January to 29.4 °C in July. High relative humidity (RH) and a large amount of rainfall occurred in August (290 mm in total), and less precipitation and low RH in autumn and winter. Wind data suggest that the prevailing wind was from northeast in winter and from east and southeast in summer (see wind-rose plot in Fig. 1a).

To further understand the general transport characteristics of air masses recorded at the site, we conducted 7 d backward particle release simulations using a Lagrangian dispersion model Hybrid Single-Particle Lagrangian Integrated Trajectory (HYSPLIT), developed in the Air Resource Laboratory (ARL) of the USA National Oceanic and Atmospheric Administration (NOAA) (Draxler and Hess, 1998). In this study, we applied the model following a method developed by Ding et al. (2013a). Briefly, for each hour during the study period, the model was run 7 d backwardly with 3000 particles released 100 m a.g.l. over the site. The spatiotemporal distributions of these particles were used to further calculate the source–receptor relationship. The residence time of particles at 100 m level was used to identify “footprint” retroplume and to calculate the potential source contribution (PSC). This method has been evaluated and has shown very good performance in the simulation of long-living species like CO, and shows wide application in understanding the transport and origins of air pollutants (Stohl et al., 2003; Cooper et al., 2005; Ding et al., 2009, 2013a). In this study, 3 h 0.5 by 0.5 degree Global Data Assimilation System (GDAS) data were used to drive the model. A high resolution emission inventory (0.2 by 0.2 degree), developed by Zhang et al. (2009), was used to calculate the PSC of CO and PM_{2.5}.

Based on a 7 d backward particle release simulation for each hour during the 1 yr study period, Fig. 2a–d give the averaged distribution of retroplumes at the site for spring, summer, autumn, and winter, respectively. These figures give clear pictures about the transport history of air masses recorded at the site. Previous studies suggested that Asian monsoon dominates the regional/long-range transport of the air pollution in East Asia (e.g., Liu et al., 2002; Naja and Akimoto, 2004). In summer and winter, the retroplumes show completely different transport patterns under the influence of the Asian monsoon (Fig. 2b and d). In summer, the air masses generally originated from the Northwest Pacific Basin and the South China Sea and were transported

Table 1. Statistics of general meteorological parameters at Nanjing for the 1 yr period August 2011–July 2012*.

Month	Pressure (hPa)	Temp (°C)	RH (%)	Rainfall (mm)
Jan	1023.7	2.9	66.1	22.6
Feb	1021.1	3.0	67.5	77.0
Mar	1016.9	9.0	67.4	83.4
Apr	1007.9	18.0	64.6	60.2
May	1006.3	21.9	65.8	62.6
Jun	1000.0	25.5	68.9	20.4
Jul	999.4	29.4	67.4	184.0
Aug	1002.3	27.0	80.2	291.1
Sep	1009.4	23.1	71.0	13.1
Oct	1016.6	17.5	69.1	29.4
Nov	1018.3	14.7	72.5	23.2
Dec	1025.9	4.2	64.8	17.0

*Note: average for pressure, air temperature, and RH, and accumulated monthly value for rainfall.

to the site by southeasterly/southwesterly summer monsoon. However, during wintertime, the air masses were generally originating from the inner Eurasian continent and transported southeasterly by the winter monsoon, resulting in a high residence time from Mongolia to the North China Plain. Associated with a continental high pressure system, those continental air masses in winter were generally transported to the site from the Yellow Sea (NE) by clockwise anti-cyclone flows. Spring and autumn are the two transition periods with air masses mainly transported from eastern China, the Yellow Sea and the East China Sea and adjacent oceans. As we show in Sect. 3.1, the distinguished transport patterns in different seasons controlled the seasonal behaviors of primary pollutants at the site. The transport patterns also indicate that the observed air masses could carry information from the entire eastern part of China and further suggest that the SORPES site could be an ideal regional background station for assessing change of atmosphere on a larger scale.

3 Results and discussions

3.1 Seasonal behaviors

With 1 yr continuous measurements for the period of August 2011–July 2012, we acquired the first picture of seasonal behaviors of O₃, PM_{2.5}, and relevant precursors in the west YRD region. Figure 3a–f give monthly variation of O₃, PM_{2.5}, SO₂, CO, NO_y, and NO, respectively.

Ozone shows a distinguished seasonal pattern, with an overall broad peak in summer and early autumn (a maximum in July and a secondary maximum in September) and a minimum in winter (November). The observed seasonal behavior of O₃ at the site is different from what has been reported in previous studies conducted in eastern and southern

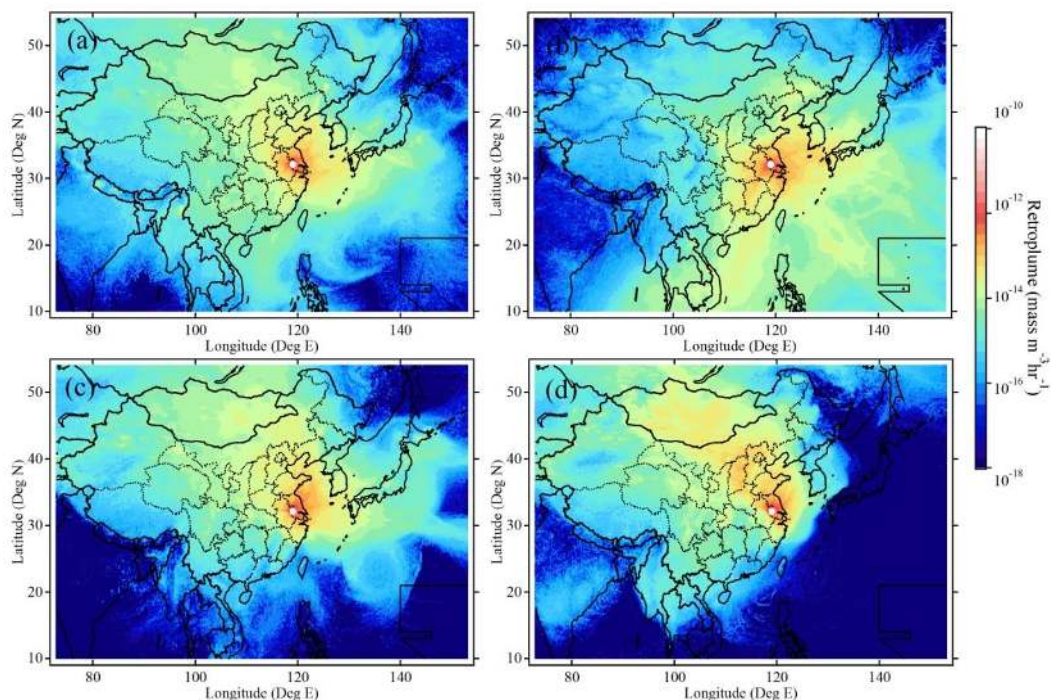


Fig. 2. Averaged retroplume (“footprint” residence time) showing transport pathways of air masses observed at Nanjing during (a) spring, (b) summer, (c) autumn, and (d) winter for the 1 yr period. Note: Red circle on the map shows the SORPES site location.

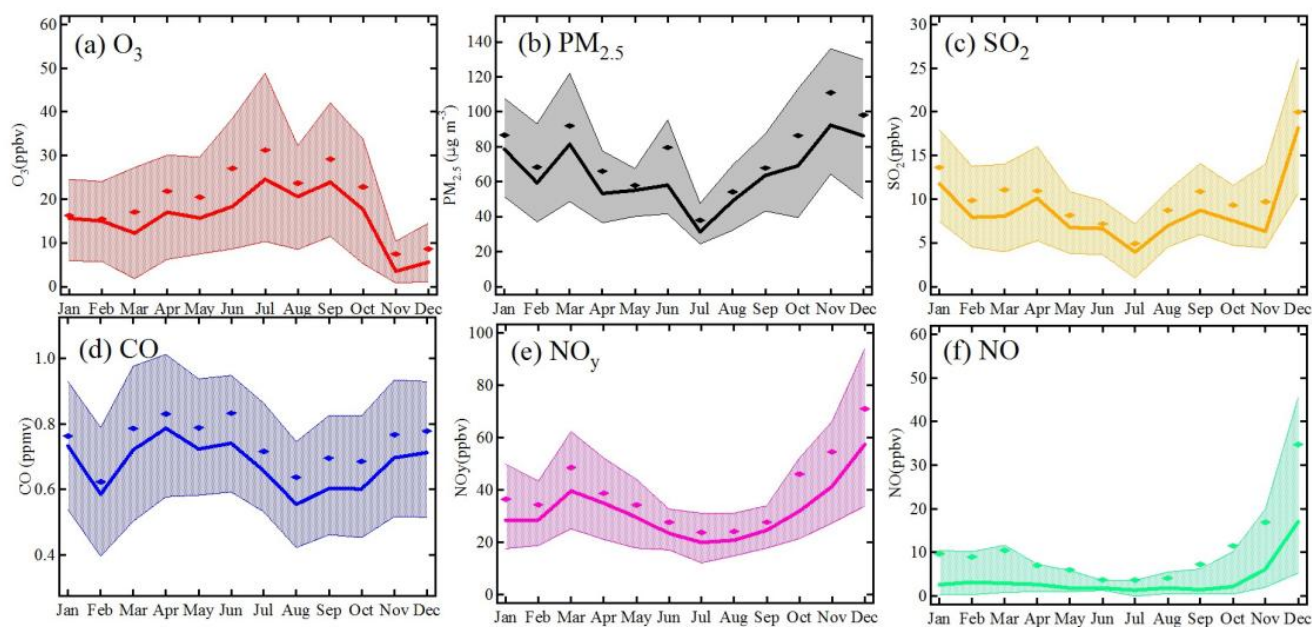


Fig. 3. Seasonal variation of (a) O_3 , (b) $PM_{2.5}$, (c) SO_2 , (d) CO , (e) NO_y and (f) NO . Bold solid lines are the median values, diamonds show the monthly averages and thin solid lines represent percentiles of 75 % and 25 %.

China. For instance, a summer minimum and autumn maximum of O_3 were recorded at Hong Kong in southern China (Wang et al., 2009), and an early summer (June) broad max-

imum of O_3 was reported in Beijing (Ding et al., 2008; Lin et al., 2008, 2009). For the YRD region, available observations from either surface measurement at Lin’an (Xu

et al., 2008) or satellite retrievals at Shanghai (Dufour et al., 2010) suggest a later spring (May) maximum and early autumn (September) secondary maximum, which was attributed to a well-defined summertime decrease of O_3 associated with “clean” maritime air transported from the Pacific Ocean by the monsoons. Considering the geographical location of Nanjing, which is downwind of the YRD under the influence of southeasterly summer monsoon, the emissions in the YRD region and the strong solar radiation might be the main causes of an O_3 formation in summer, resulting in a different seasonal cycle of O_3 compared to other coastal sites in the east/southeast YRD. In fact, the CO and NO_y data (Fig. 3d–f) show that these precursors were still at fairly high levels (about 600 ppbv and 25 ppbv, respectively) in summer.

For the fine particle $PM_{2.5}$, Fig. 3b shows an overall well-defined seasonal pattern with a maximum in autumn (November) and a minimum in summer (July). This clear seasonal pattern could be due to the change of emission, deposition and vertical mixing processes in different seasons. Emission of particulate matter is generally high in cold seasons because heating in northern China requires more consumption of fossil fuels (Zhang et al., 2009) and in winter the dry weather and strong winds contribute to increased particle suspension and advection. Deposition should also have a strong seasonal variation because high precipitation (Table 1) favors wet-deposition and high soil humidity, and the growth of deciduous plants may enhance the dry deposition of particular matter in warm seasons (Zhang et al., 2001). The relatively low concentration of $PM_{2.5}$ in summer may be also partly due to an increased vertical mixing (i.e., a higher boundary layer height) and more convection in that season (Ding et al., 2009). $PM_{2.5}$ mass concentration also showed strong month-to-month variations, e.g., a sharp peak in June and a drop in February. The June peak was mainly associated with intensive activities of straw burning, as we discuss in Sect. 3.3. The drop of $PM_{2.5}$ concentration together with other primary pollutants, such as SO_2 , CO and NO_y , in February is attributed mainly to the winter break of the Chinese Spring Festival, which started at the end of January and lasted until mid-February.

Other primary trace gases all show dramatic seasonal cycles but also some unique month-to-month variation patterns. For instance, NO_y concentration increased at the end of autumn, with a maximum appearing in December together with a sharp peak of NO. Examination of the time series suggests that in December there was a multi-day episode of NO with mixing ratio up to 300 ppbv and these episodes were generally associated with northwest wind, suggesting a fresh emission from factories in the industrial zone in the northwest. The high NO concentrations also cause titration of O_3 in November and December (Fig. 3a). SO_2 concentration shows a strong increase in winter but a significant drop in November. The drop was associated with the $PM_{2.5}$ maximum and a relatively high RH (Fig. 3b and Table 1), suggesting a possible role of heterogeneous reactions (Ravishankara, 1997). In

fact, in this region a high frequency of fogs generally occurs in autumn, especially in November.

3.2 Inter-species correlations

Investigation of correlations between different species was done to help interpret the data and gain some insights into the related mechanisms/processes. In Fig. 4a–e, we give scatter plots of O_3 – NO_y , SO_2 – NO_y , CO– NO_y , $PM_{2.5}$ – O_3 and $PM_{2.5}$ – NO_y , respectively. To differentiate the correlations under the influence of relevant meteorological/environmental factors, the data points are color-coded with different parameters (e.g., air temperature, relative humidity and O_3 mixing ratio).

Figure 4a shows that O_3 measured at the site has an overall negative correlation with NO_y . The color of data points shows that the negative correlation mainly exists for data of low air temperature, suggesting a titration effect of freshly emitted NO with O_3 in cold seasons and at nighttime. In contrast, a positive correlation between O_3 – NO_y prevailed during high air temperature, which mainly appeared in daytime of warm seasons with a moderate level (<100 ppbv) of NO_y . These results suggest a strong photochemical production of O_3 in this region in summer, resulting in the seasonal cycle pattern of O_3 shown in Fig. 3a.

The two primary pollutants SO_2 and NO_y show a quite good correlation (Fig. 4b). However, the SO_2/NO_y ratio obtained from this study is much lower than levels previously reported at Lin’an ten years ago (e.g., Wang et al., 2004). This can be explained by a significant reduction of SO_2 emission from power plants but an increased NO_x emission associated with a huge consumption of petroleum fuels in the past decade in this region (Richter et al., 2005; Zhang et al., 2009). The color of data points given in Fig. 4b shows an obvious relationship between RH and SO_2/NO_y ratio. A better correlation and a higher SO_2/NO_y ratio is obtained for air with low humidity, while for the humid air masses the relationship is much more scattered, and the ratio of SO_2/NO_y is clearly low, suggesting a higher conversion of SO_2 to sulfate and/or deposition in the humid environment (Khoder, 2002).

A scatter plot of CO– NO_y given in Fig. 4c is color-coded with O_3 concentration. It shows that high O_3 levels are generally associated with air masses of high CO/ NO_y ratio. For NO_y lower than 100 ppbv, an increase of CO always results in higher O_3 concentration, but NO_y reverses. As volatile organic compounds (VOCs) generally have good correlation with CO and play a similar role as CO in the photochemical ozone production (Atkinson, 2000), the O_3 –CO– NO_y relationship strongly indicates a VOCs-limited regime of O_3 formation in this region. Geng et al. (2008) also reported a VOCs-limited regime in Shanghai by using measured and modeling results. It needs to be pointed out that even though NO_x control policies have been implemented in China, our results suggest that an inappropriate control of NO_x alone may lead to increased O_3 pollution for the YRD region.

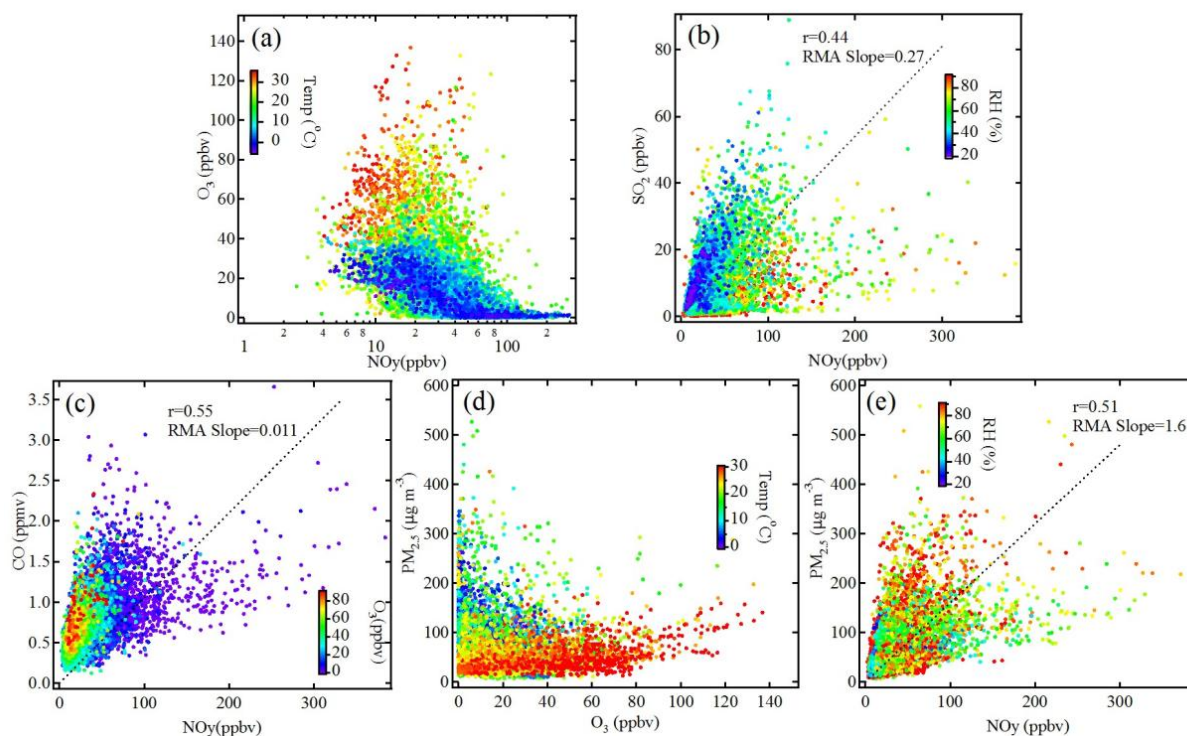


Fig. 4. Scatter plots of (a) O_3 – NO_y color-coded with air temperature, (b) SO_2 – NO_y color-coded with relative humidity, (c) CO – NO_y color-coded with O_3 concentrations, (d) $\text{PM}_{2.5}$ – O_3 color-coded with air temperature, and (e) $\text{PM}_{2.5}$ – NO_y color-coded with RH.

Figure 4d gives a scatter plot of $\text{PM}_{2.5}$ and O_3 color-coded with air temperature. Interestingly, a negative correlation can be found for low air temperature samples but a pronounced positive correlation existed for high temperature data points. The anti-correlation for cold air could be mainly attributed to the titration effect of high NO concentration, which was associated with high primary $\text{PM}_{2.5}$ in cold seasons, and the positive correlation with an increasing slope indicates a formation of secondary fine particles in summer associated with high concentration of O_3 . Here the secondary particle formation may be related to high conversion rate of SO_2 to sulfate under a high concentration of oxidants (Khoder, 2002). It may also be related to formation of secondary organic aerosols with high O_3 concentrations (Kamens et al., 1999) because biogenic emission of VOCs could also be high in the upwind rural area under a condition of high air temperature and solar radiation in summer. Previous studies of $\text{PM}_{2.5}$ chemical compositions in Shanghai and Nanjing (e.g., Wang et al., 2002, 2006) and an intensive measurement of water soluble ions at the SORPES station (Ding et al., 2013b) all suggested that sulfate was the most dominate ion in $\text{PM}_{2.5}$. The detailed mechanisms still need to be further addressed by long-term measurement of aerosol chemical composition.

Figure 4e shows a good positive correlation between $\text{PM}_{2.5}$ and NO_y . It suggests that the $\text{PM}_{2.5}$ at the site was mainly associated with combustion sources. Some green data

points in the plot show very high NO_y concentration associated with relatively low $\text{PM}_{2.5}$. These data were corresponded with the extremely high NO plumes in December, which, as mentioned above, came from the nearby factories in the northwest. Figure 4e also shows that high RH data are very scattered but do not show a systematic high $\text{PM}_{2.5}/\text{NO}_y$ ratio, indicating that the influence of humidity to SHARP $\text{PM}_{2.5}$ measurement was not significant during the study period, even under the high RH condition in summer.

3.3 Discussions on O_3 and $\text{PM}_{2.5}$ episodes

3.3.1 Overall statistics of exceedances to standards

The above analysis has shown overall high O_3 concentrations in summer and high $\text{PM}_{2.5}$ levels during the entire year, with extremely high $\text{PM}_{2.5}$ concentrations in the cold seasons. To further understand the air pollution situation, Table 2 gives statistical information of O_3 and $\text{PM}_{2.5}$ mass concentrations with a comparison to the National Ambient Air Quality Standards in China (NAAQS-CN), which were released in early 2012 by the China State Council and will be implemented nationwide in 2016 (MEP, 2012). According to the Class II NAAQS for O_3 ($160 \mu\text{g m}^{-3}$ for 8 h average and $200 \mu\text{g m}^{-3}$ for 1 h average), there were 15 days of O_3 exceedances in total during the 1 yr period, which mostly occurred in warm seasons (June–October). This frequency is

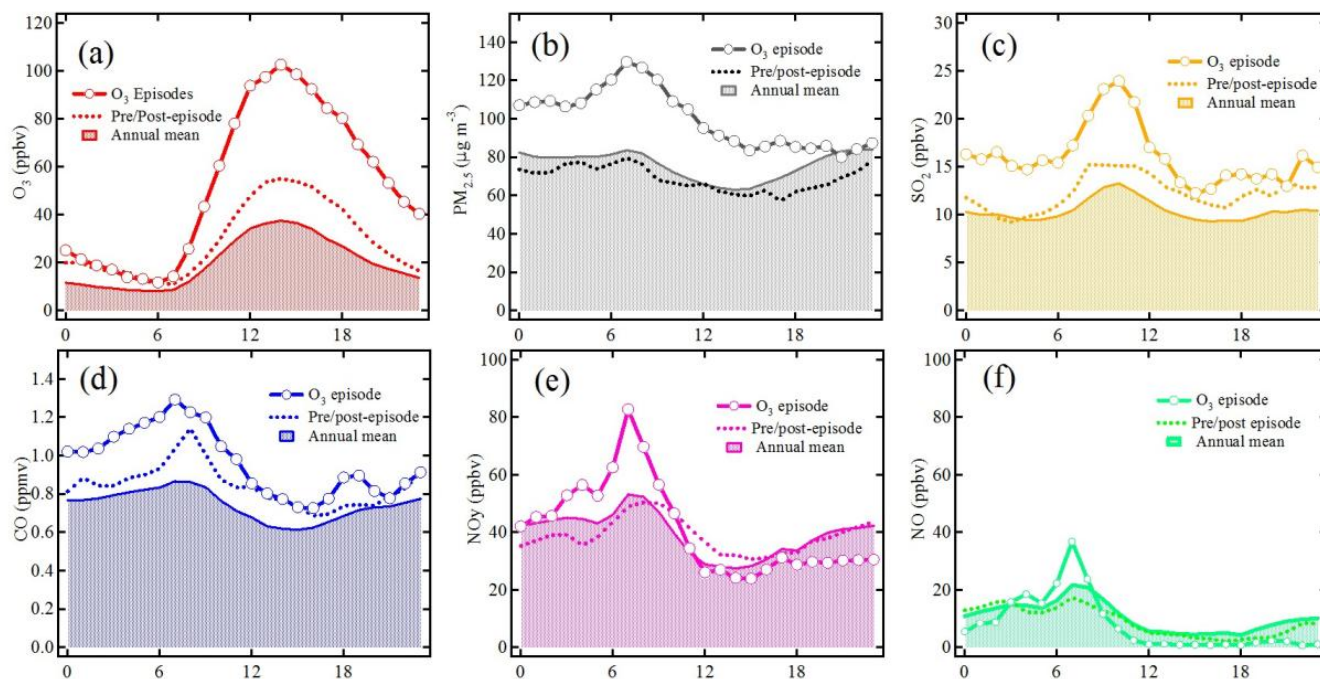


Fig. 5. Diurnal variations of (a) O₃, (b) PM_{2.5}, (c) SO₂, (d) CO, (e) NO_y, and (f) NO, averaged for O₃ episode days with exceedances of the NAAQS-CN and the pre-/post-episode days during the entire 1 y period.

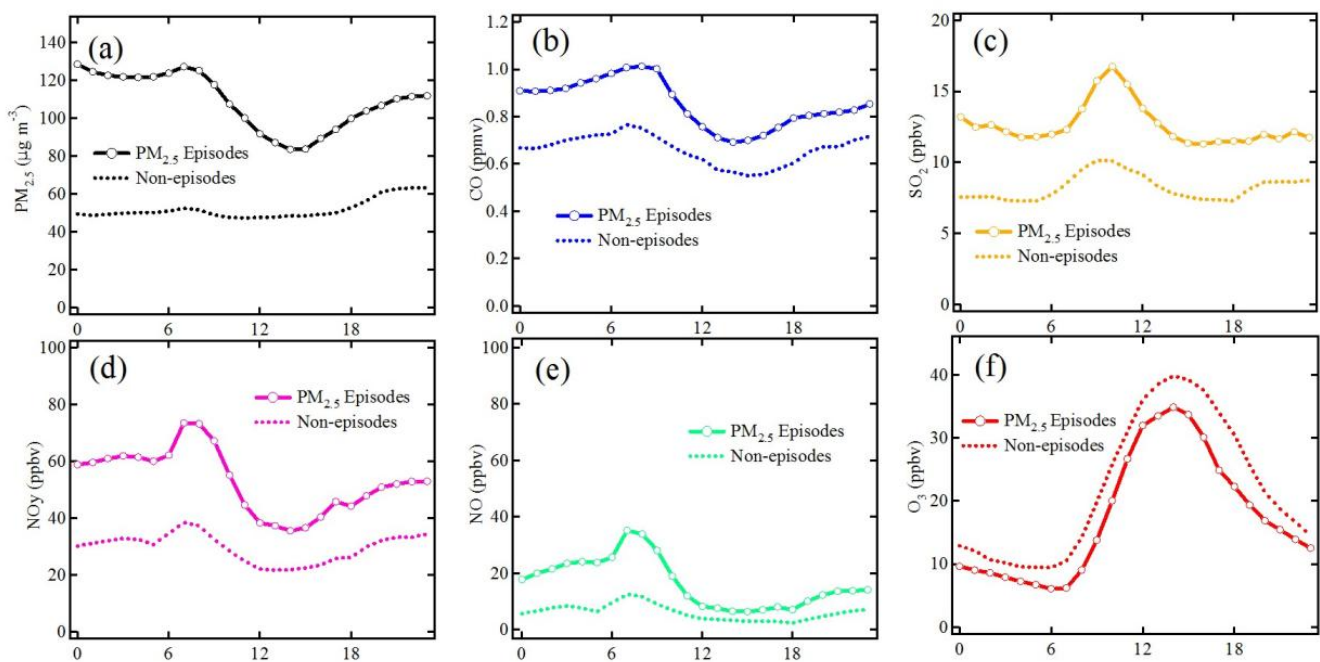


Fig. 6. Diurnal variations of (a) PM_{2.5}, (b) CO, (c) SO₂, (d) NO_y, (e) NO, and (f) O₃, averaged for PM_{2.5} episode days with exceedances of the NAAQS-CN and the non-episode days.

Table 2. Monthly statistics of average, maximum and number of exceedances of O₃ and PM_{2.5} compared with the National Ambient Air Quality Standards in China.

Month	O ₃ (mg m ⁻³)			PM _{2.5} (μg m ⁻³)		
	Mean	Max ¹	N.o.E. ²	Mean	Max ¹	N.o.E. ²
Jan	31.9	111.1	0	86.8	278.0	19
Feb	30.4	78.4	0	68.4	276.8	12
Mar	33.5	221.8	1	92.0	301.0	18
Apr	42.8	189.6	2	66.1	322.3	8
May	40.0	167.6	0	58.0	198.7	6
Jun	53.1	267.9	3	79.7	425.6	13
Jul	61.3	236.7	3	38.0	115.8	1
Aug	46.4	223.1	2	54.3	177.1	3
Sep	57.2	213.2	2	67.9	226.5	10
Oct	44.7	259.9	2	86.4	425.0	17
Nov	14.6	105.4	0	111.0	558.3	21
Dec	16.9	62.8	0	98.2	391.8	20
Annual	39.4	267.9	15	75.6	558.3	148

¹Max means a maximum of hourly concentration.

²N.o.E. of O₃ accounts for days with 1 h or 8 h average exceed the Class II NAAQS-CN (160 and 200 μg m⁻³ for 8 h and 1 h average, respectively). N.o.E. of PM_{2.5} accounts for days with 24 h average over 75 μg m⁻³.

higher than that observed in Shanghai by Ran et al. (2012). For PM_{2.5}, the annual averaged concentration is 75.6 μg m⁻³, more than twice the annual standard (35 μg m⁻³), and 148 days (40 % of the year, mainly in cold seasons from September to June) exceeded the daily limit of 75 μg m⁻³. It is noteworthy that the annual mean PM_{2.5} concentration is almost equal to the estimation given by van Donkelaar et al. (2010), which suggested a multi-year average of PM_{2.5} mass concentration over 80 μg m⁻³ in eastern China by using satellite data during 2001–2006. As our measurements were conducted upwind of Nanjing, the results show a severe regional air quality problem in the YRD.

To help understand the causes of O₃ episodes, in Fig. 5 we give the averaged diurnal patterns of O₃, PM_{2.5} and related species for the 15 days with O₃ exceedances, together with those for 1 day before and after those exceedances, as well as the annual means. O₃ shows a typical diurnal cycle with a minimum in the early morning and the daily maximum in the early afternoon (~14:00 LT). However, during the episode days, O₃ concentration experienced a dramatic daytime buildup (about 50 ppbv higher than pre-/post-episode days), suggesting very strong in situ photochemical production. For O₃ precursors and PM_{2.5}, their diurnal cycles in either episode days or non-episode days all show a morning peak (Fig. 5d–f) and an afternoon dip. These patterns are mainly related to the evolution of the boundary layer (PBL) since there are only a few local sources in this region. The morning peaks could be related to a nighttime accumulation of primary pollutants within the nocturnal PBL, and the concentrations dropped gradually as the daytime PBL developed after sunrise. As SO₂ is mainly emitted from elevated sources

like power plants, it shows a delayed peak around 10:00 LT, i.e., a time with PBL mixing height well developed, suggesting a possible fumigation of residual layer pollution. A similar phenomenon of SO₂ has also been reported at Lin'an and Beijing (Wang et al., 2004, 2006). Comparison of the diurnal patterns for episode and non-episode days also shows higher concentrations of O₃ precursors, PM_{2.5} and SO₂ on episode days, particularly in the early morning, suggesting an important contribution of in situ photochemical production in a mixed plume. Another interesting point is that aerosols are generally considered as a constrain factor to O₃ production as they can affect actinic flux of UV radiation (Dickerson et al., 1997), but here we cannot see such an effect as PM_{2.5} was also well-correlated with O₃ precursors.

Similar to Fig. 5, Fig. 6 gives statistical information of diurnal variations of PM_{2.5}, CO, SO₂, NO_y, NO, and O₃ for the days of PM_{2.5} exceedances (40 % of the year) and non-exceedance days. PM_{2.5} in the episode days shows dramatically higher concentrations and stronger diurnal variability than in the non-episode days, while the trace gases show similar diurnal patterns but about 20–40 % higher concentrations during episode days. The higher difference of PM_{2.5} in early morning of the episode days might be related to primarily emitted sources, which could be higher in dry cold seasons because of higher emission rate and lower nocturnal PBL height. On the other hand, since the non-episode days were mainly in warm seasons, a relatively higher soil humidity and consequently much denser foliage of the plants could also cause a higher deposition rate, resulting in less accumulation of primary aerosols in the boundary layer. The missing afternoon dip of PM_{2.5} for non-episode days might be due to the formation of secondary aerosols, as discussed in Sect. 3.2. The O₃ diurnal patterns given in Fig. 6 show higher O₃ levels for the entire period of non-episode days, which indicates favorable conditions for the formation of secondary particles. In fact, from the SO₂ diurnal pattern of non-episode days, a notable drop of SO₂ concentration associated with the O₃ peak may also indicate such an increased conversion.

3.3.2 Case studies for high O₃ and PM_{2.5} episodes

To further understand the main causes – including weather and transport characteristics – of high O₃ and PM_{2.5} episodes, four typical episodes were selected for detailed case studies and are presented below.

- Case I: mixed high O₃/PM_{2.5} related to anticyclones. Fig. 7a presents a case of high O₃ and PM_{2.5} episode that occurred during the period of 7–10 October 2011. It shows that high O₃ (up to 140 ppbv) occurred on 7 October and broad O₃ peaks (up to 90 ppbv) appeared in the following two days. PM_{2.5} and primary pollutants (SO₂, CO and NO_y) also reached very high levels on 7 October. Examining weather charts for the period suggests that a stagnant high pressure system dominated

Table 3. Estimation of regional contribution of CO and PM_{2.5} to the SORPES site during the 1 yr period.

Region	CO (ppm)			PM _{2.5} (μg m ⁻³)		
	O ₃ Episode	Pre-/Post-O ₃ episode	Annual Rate	Episode	Non-episode	Annual Rate
YRD	0.632	0.547	72.1 %	51.6	38.8	69.0 %
M.YRD	0.548	0.414	59.7 %	39.3	30.0	53.0 %

central and eastern China for a few days, with its center located over the YRD on 7 October (see Fig. 7b). The averaged 7 d backward retroplume for the period of 7–9 October clearly shows a clockwise anticyclone flow and a long residence time over the YRD region, especially over the city clusters along the Shanghai–Nanjing axis corresponding to Fig. 1c. For the first day of the episode (7 October), the highest O₃ together with high PM_{2.5} and primary pollutants CO, SO₂ and NO_y suggests a strong in situ photochemical production in mixed regional plumes under the influence of anticyclones. In the following two days, continuous maritime air from the East China Sea and the Northwest Pacific Basin in the east, which brought relatively fresh emission from the YRD region (Fig. 7c), also produced high O₃ concentration up to 90 ppbv. PM_{2.5} mass concentration remained over 100 μg m⁻³ while CO, NO_y and SO₂ concentrations were moderate. In this case, the anticyclones (i.e., high pressure) caused favoring conditions, e.g., sunny weather and low wind velocities, for pollution accumulation and O₃ production. A similar relationship between high pressure and O₃ episodes has been reported elsewhere (e.g., Luo et al., 2000; Hegarty et al., 2007; Guo et al., 2009). These results clearly demonstrate a case of sub-regional transport of primary and secondary air pollutants within the YRD region under the influence of anticyclones.

- Case II: high PM_{2.5} before the passage of a cold front. At the end of November 2011, an extremely high concentration PM_{2.5} episode was observed at the site, with PM_{2.5} mass concentration raised over 500 μg m⁻³ (Fig. 8a). Weather charts show that this case occurred under calm conditions before the passage of a strong cold front, which was at the front of a strong continental high pressure system originating from Mongolia and sweeping over Nanjing in the early morning of 30 November (see Fig. 8b). On 28 November, weak easterly and southeasterly winds dominated the YRD region, which brought pollutants from the city clusters to the site (see the average retroplume given in Fig. 8c). In contrast to Case I with the influence of dominant anticyclones, no high O₃ concentration was observed in this case, which may be due to the strong titration effect of high NO (see Fig. 8a) and weak solar radiation. It is also

worthwhile to point out that most of the species showed a significant drop but O₃ rose to about 20 ppbv after the passage of the cold front on 30 November. Wind data suggest a strong northeast flow passing over the Yellow Sea from the north, with air masses representing the continental background from high latitudes. This phenomenon is quite different from that observed in southern China, where cold fronts have generally brought polluted continental outflows from eastern China and caused a sharp increase of primary plumes during and after the passage of the cold front (Wang et al., 2003). Besides the effect of transport, this case also shows the effect of wet deposition on some pollutants. For example, a significant drop of PM_{2.5} (to as low as 10 μg m⁻³) and SO₂ seems to be associated with precipitation after the passage of the cold front (see Fig. 8a).

- Case III: high PM_{2.5} and O₃ related to biomass burning. As we mentioned in the introduction, eastern China is the most important agricultural base in China, with wheat and rice production alternating in cold and warm seasons. In the last decades, burning of crop straw has been intensive during the harvest period. Ding et al. (2013b) reported an outstanding case observed in mid-June 2012 at the SORPES site and found that episodes of extremely high PM_{2.5} concentrations could substantially modify the weather. Here we further discuss air pollution transport for this case. The time series given in Fig. 9a shows extremely high PM_{2.5} mass concentrations observed during the period of 9–10 June and a multi-day episode of high O₃ occurring during the following days. Based on PM_{2.5} chemical composition, Ding et al. (2013b) clearly demonstrated that the high PM_{2.5} air masses were caused by straw burning plumes mixed with fossil fuel combustion pollutants. Figure 9d further confirms the transport pathway of such an episode and clearly shows that the observed air masses were associated with long residence time over the burning area and polluted region around Nanjing. On 10 June 2011, a low pressure was located in the west of Nanjing. Because of high NO concentrations and low solar radiation due to extremely high PM_{2.5} concentrations, O₃ concentrations dropped to almost zero. However, two days after the episode, O₃ increased to values over 120 ppbv during the period of 12–14 June.

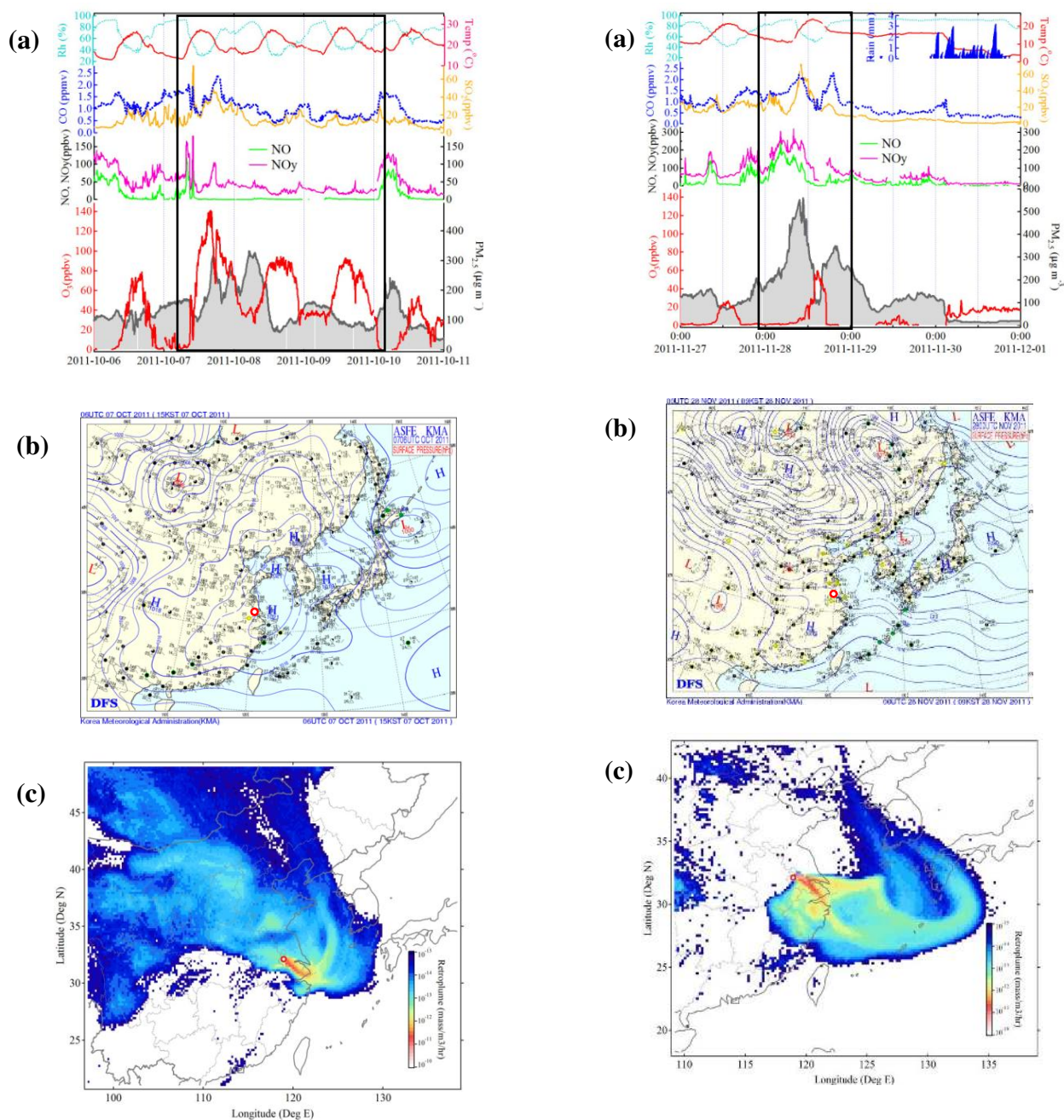


Fig. 8. Same as Fig. 7 but for Case II, i.e., 27–30 November 2011.

Fig. 7. (a) Time series of O_3 , $PM_{2.5}$, related trace gases and meteorological parameters for Case I, i.e., 6–10 October, 2011. (b) Weather chart on 7 October 2011. (c) Averaged retrorplume of air masses at Nanjing for the period indicated at bottom of (a). Note: The red circle in (b) and (c) shows SORPES site location.

Again, the synoptic weather shows an anticyclone located over the YRD (see Fig. 9c), and the averaged retrorplume and trajectories clearly indicate that the high O_3 concentrations were associated with aged biomass burning plumes mixed with anthropogenic pollutants in

the southern part of YRD after being re-circulated back from the sea east of the YRD (see Fig. 9e).

- Case IV: multi-day episode of high O_3 and secondary $PM_{2.5}$. This case shows a multi-day episode of O_3 and $PM_{2.5}$ observed during the period of 5–25 July 2012. Figure 10a shows that O_3 concentrations experienced very strong diurnal cycles within these ten days, with daytime maximum O_3 concentrations over 120 ppbv on 16, 19, and 20 July. Examination of day-by-day weather

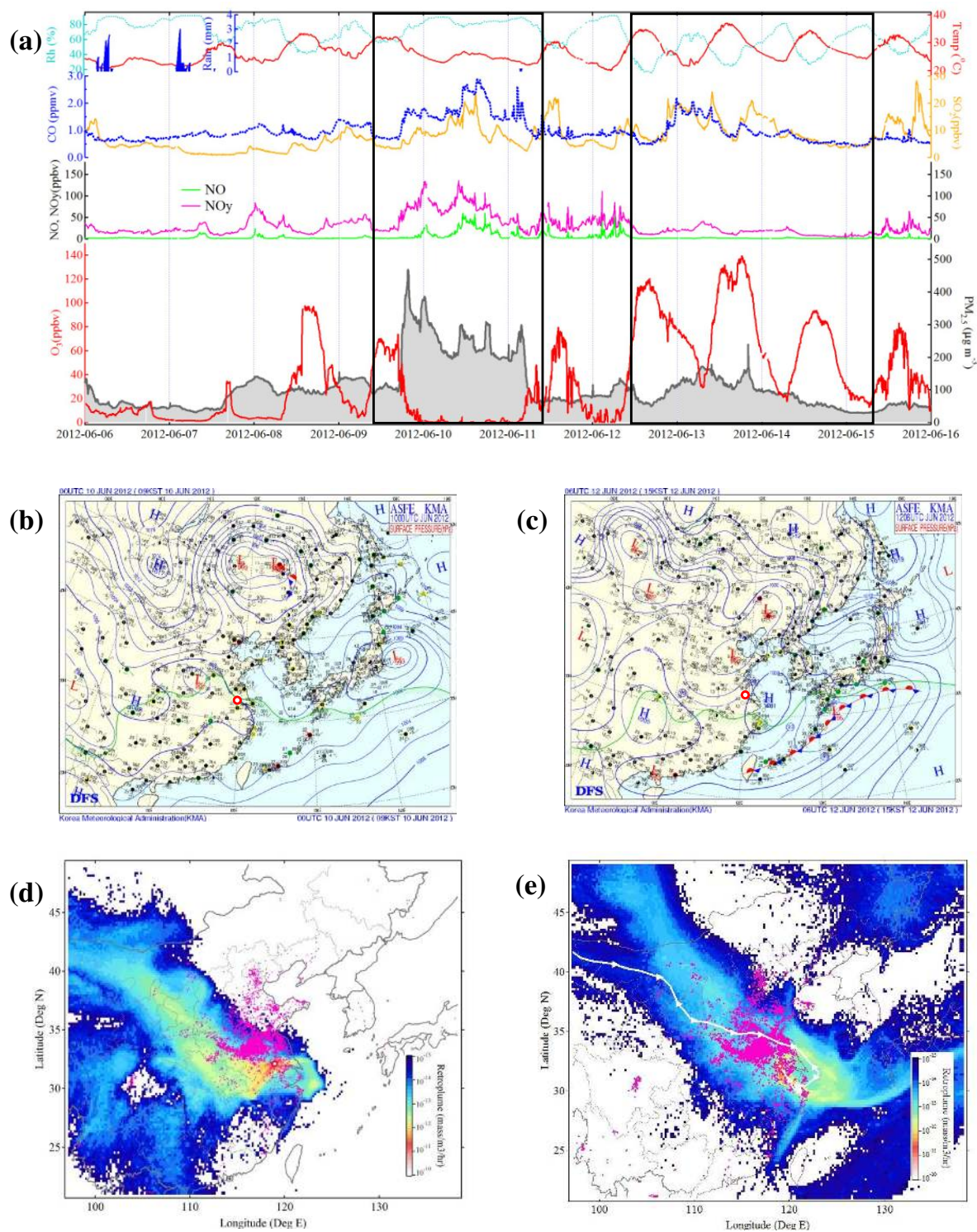


Fig. 9. (a) Time series of O₃, PM_{2.5}, related trace gases and meteorological parameters for Case III, i.e., 9–15 June, 2012; and weather charts for (b) 10 June 2011 and (c) 12 June 2011. (d) Averaged retrorplumes for the periods marked with black boxes in (a), and (e) with pink points in (a), give MODIS fire accounts for the period of 6–13 June 2012. White line with triangles given in (e) shows 7 d backward trajectory for 15:00 LT on 13 June 2012.

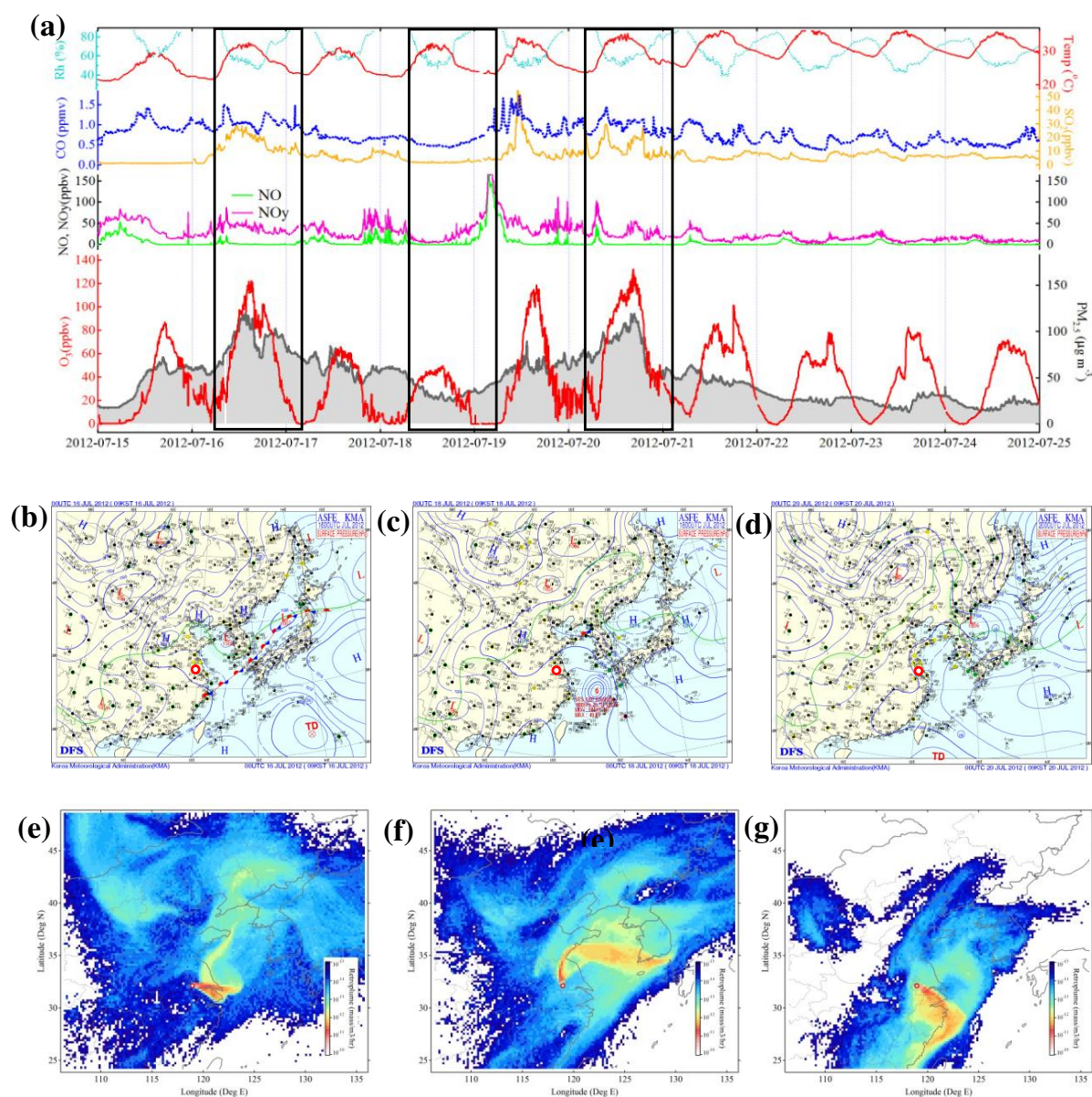


Fig. 10. (a) Same as Fig. 9a but for Case IV, i.e., 15–25 July 2012; (b–d) and (e–g) show weather charts and averaged retroplumes for the three periods marked in (a).

charts suggests that the evolution of O_3 concentrations was closely related to the change of synoptic weather. On 16 July, a front extended from southeast China to South Korea, with northern and eastern China being dominated by high pressure. Under such conditions, air masses recorded at the site show clear contributions from the city clusters in the YRD region. On that day, a tropical depression (TD) was forming in the Northwest Pacific Basin (see Fig. 10b). The TD further developed into a typhoon (No. 7, Typhoon Khanun) and its center moved to a location a few hundred kilometers southeast of the YRD on 18 July (Fig. 10c). The ty-

phoon circulation caused a strong anti-clockwise transport of air masses from the ocean (see Fig. 10f), causing a decrease of O_3 , $PM_{2.5}$, and primary pollutants on 18 July. However, in the following two days, a subtropical Pacific High dominated the Northwest Pacific Basin as the typhoon weakened and disappeared after landing in Korea. Under such conditions, the air masses recorded at the site mainly came from southeast China and swept again over the most polluted YRD city clusters in the southeast. After this episode, strong southeasterly maritime air continuously controlled eastern China, and daily maximum O_3 remained at high levels

even with low concentrations of precursors, suggesting high photochemical production efficiency of O_3 in this region in summer. In this case, $PM_{2.5}$ on 16 and 20 July also showed some indications of secondary aerosol formation. During the two days, $PM_{2.5}$ mass concentration showed very good correlation with O_3 but not with primary pollutants CO , NO_y and SO_2 , and SO_2 mixing ratios were relatively high, between 10 and 50 ppbv. As mentioned above, SO_2 can be easily converted to $PM_{2.5}$ sulfate in an environment of high concentration of oxidants and high air temperature. Besides oxidation of SO_2 , the formation of secondary aerosols may also have included contributions from biogenic emissions (VOC) because of high biomass production in this region in summer, especially in the southern part of the YRD.

3.4 Cross-boundary transport and implications for air pollution control measures

The above results have shown an important role of sub-regional transport, especially the emissions from the YRD, on O_3 and $PM_{2.5}$ pollution in the study region. To get a more holistic understanding about the regional transport, we carried out further calculations of potential source contributions (PSC) of the O_3 precursor CO and $PM_{2.5}$ for the measurements based on the Lagrangian dispersion simulations (Ding et al., 2013a). Figure 11 gives the maps of averaged PSC of CO for all the 15 episode days, in which O_3 mixing ratios exceeded the Class II NAAQS-CN, and the 20 pre-/post-episode days (i.e., one day before or after the 15 episode days). The super-regional distributions of PSC of CO for episode and non-episode days show quite small differences (Fig. 11a and b), with high contributions from the eastern part of China, particularly the YRD region. However, the zoomed view of the PSC maps for the YRD suggests completely different transport patterns. For O_3 episode days, the mid-YRD, i.e., the area along the Nanjing and Shanghai axis with its city clusters, is the main potential source region, but non-episode days show a distinct pattern with main source regions in the north YRD and only rarely from the mid-YRD cities. These results clearly demonstrate that the mid-YRD city cluster is the major source region for high O_3 pollution in upwind Nanjing. It needs to be mentioned that Ran et al. (2012) suggested that in the YRD megacity Shanghai, the O_3 pollution mainly appeared on the urban scale, but here in the western YRD region our results clearly show an important impact of regional photochemical pollution.

Figure 12 presents the same calculations for $PM_{2.5}$ exceedance and non-exceedance days. A comparison of Fig. 12a,b shows large differences in PSC on the super-regional scale. During episode days, sources have been identified to be located on the North China Plain and generally more inland areas, while for non-episode days, the main source regions form a band covering the eastern part of China, from southern China to northern China, suggesting

an important role of long-range transport on $PM_{2.5}$ pollution in Nanjing. The zoomed PSC maps show similar patterns but with obviously lower contributions for non-episode days, and a strong impact from the mid-YRD and north YRD. Figure 12c,d show high contributions of sources in the region about 20–60 km northeast from the site, which belongs to Zhenjiang City with relatively high PM emissions. It should be pointed out that the PSC of $PM_{2.5}$ only gives a “rough” estimation of the potential source region from primary sources, since the formation of secondary aerosols and removal processes like deposition have not been included. Nevertheless, this analysis does provide some consistent and valuable insights into cross-boundary transport in the YRD region.

To further gain quantitative understanding of cross-boundary sub-regional transport, in Table 3 we give statistics of regional contributions of CO and $PM_{2.5}$ from the entire YRD and mid-YRD regions. For the 1 yr average, emissions from the YRD and mid-YRD account for 72 % and 60 % of CO , and 69 % and 53 % of $PM_{2.5}$ to the site, respectively. For O_3 episode days, the YRD, especially the mid-YRD, shows a much higher contribution than non-episode days. For $PM_{2.5}$, though the relative contributions from YRD and mid-YRD regions were of a high proportion, there was much more influence from the YRD on episode days. These results suggest a substantial contribution of sub-regional/cross-boundary transport on air quality at the site. However, currently in China air pollution control measures are implemented relatively independently by local governments. For the YRD region, composed of over ten cities belonging to two provinces, Jiangsu and Zhejiang, and the municipality of Shanghai, it is a challenge for policy makers to establish collaborative control measures across administrative borders. Nevertheless, this is a critically important and urgent task to improve air quality in the inland downwind cities in the YRD (and beyond), such as Nanjing.

4 Summary

In this study, we present an overview of 1 yr measurements of O_3 and $PM_{2.5}$ as well as related precursors at the regional background station SORPES in Nanjing, an inland YRD city in eastern China. The characteristics and causes of O_3 and $PM_{2.5}$ concentrations are discussed by investigations of temporal variations, inter-species correlations, and case studies based on weather data and Lagrangian dispersion modeling. The main findings and conclusions are summarized as follows:

1. Both O_3 and $PM_{2.5}$ had distinguished seasonal variations during the 1 yr study period. O_3 showed a maximum in July and a secondary peak in September, while $PM_{2.5}$ reached maximum values in November and a minimum in July. Within the 1 yr measurement period, there were 15 days of O_3 exceedance and 148 days (40 %) of $PM_{2.5}$ exceedance of the National Ambient

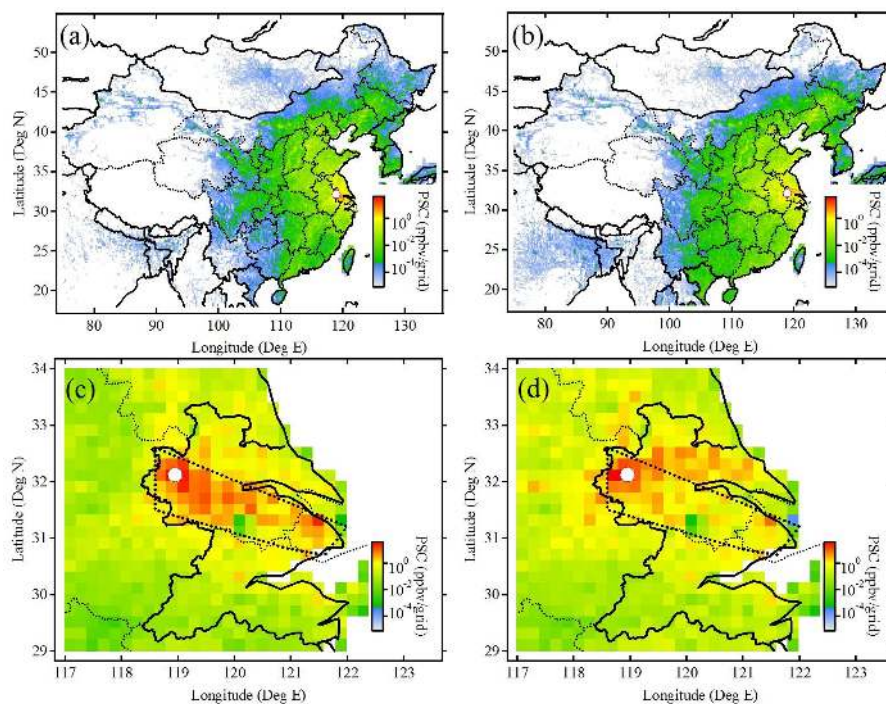


Fig. 11. (a) and (b) are averaged distributions of potential source contribution of CO for episode days with O₃ exceedances and pre-/post-episode days, respectively. (c) and (d) are zoomed views of (a) and (b), respectively. Note: the dashed line shows the mid-YRD area.

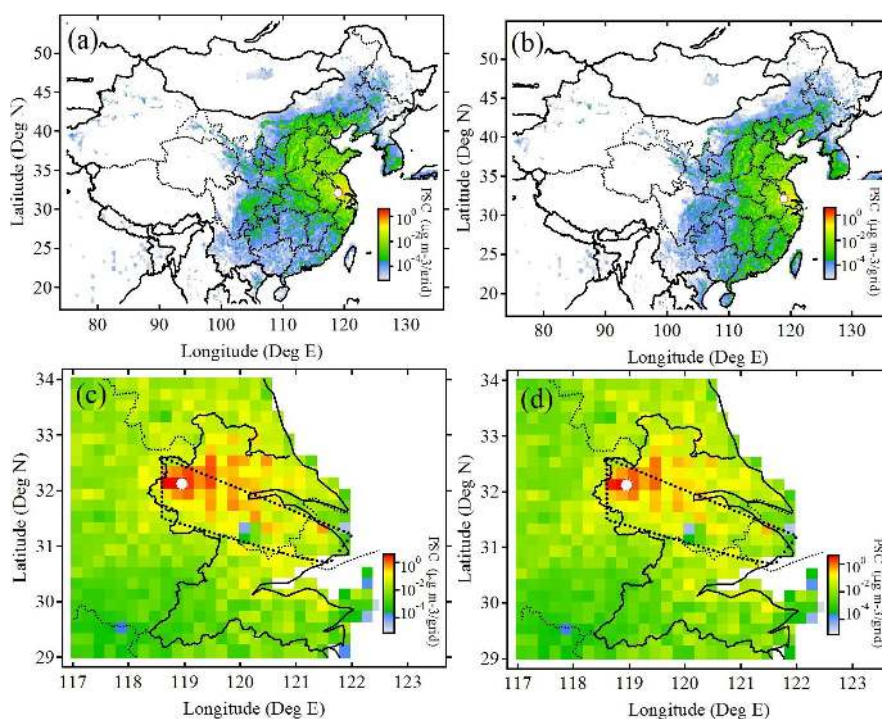


Fig. 12. Same as Fig. 11 but for days with PM_{2.5} exceedances and non-episode days, respectively.

Air Quality Standards in China at the site, suggesting heavy air pollution in this region.

- Correlation analysis shows a positive O_3 – NO_y correlation for air masses with high air temperature in summer but a negative one in winter, and shows a significant conversion or deposition of SO_2 under humid conditions. CO – NO_y – O_3 correlations indicate a VOC-limited regime for photochemical production of O_3 in this region, and $PM_{2.5}$ – O_3 correlations demonstrated the formation of secondary aerosols under conditions of high O_3 in summer.
- Case studies for typical O_3 and $PM_{2.5}$ episodes with exceedance of national air quality standards suggest an important influence of air pollutants emitted from the mid-YRD, i.e., the Nanjing–Shanghai axis with its city clusters in between. Synoptic weather plays an important role in the development of these episodes, and O_3 episodes are generally associated with anticyclones. Emissions from agricultural burning in this region can cause a significant rise in $PM_{2.5}$ and O_3 concentrations during the harvest seasons.
- Calculations of potential source contributions suggest that emissions from the YRD, especially the mid-YRD, contributed a majority of the CO (over 60 % on average) at the site. For $PM_{2.5}$, the emissions from the northern part of the YRD, mainly nearby Zhenjiang City, and the entire North China Plain are the main contributors.

This work highlights the important environmental impact from human activities in the YRD region, and suggests that collaborative control measures among different administrative regions are urgently needed to improve air quality in the western part of YRD region.

Acknowledgements. The analysis of this study was supported by National Basic Research Project (973 Project 2010CB428503) and National Natural Science Foundation of China (D0512/41075010). Part of the activities was also supported by the Academy of Finland projects (1118615, 139656) and the European Commission via ERC Advanced Grant ATM-NUCLE. The SORPES station was funded by 985 Fund and Basic Research Funds from Central Universities of Ministry of Education. The authors would like to thank P. Hari at University of Helsinki and iLEAPS SSCs for their advice on developing the SORPES station, and thank T. Wang at The Hong Kong Polytechnic University and W. Wang at Shandong University for their support for the measurements and for suggestions on the data analysis.

Edited by: P. Artaxo

References

- Allen, R. J., Sherwood, S. C., Norris, J. R., and Zender, C. S.: Recent Northern Hemisphere tropical expansion primarily driven by black carbon and tropospheric ozone, *Nature*, 485, doi:10.1038/nature11097, 350–353, 2012.
- Atkinson, R.: Atmospheric chemistry of VOCs and NO_x , *Atmos. Environ.*, 34, 2063–2101, doi:10.1016/S1352-2310(99)00460-4, 2000.
- Chameides, W. L., Yu, H., Liu, S. C., Bergin, M., Zhou, X., Mearns, L., Wang, G., Kiang, C. S., Saylor, R. D., Luo, C., Huang, Y., Steiner, A., and Giorgi, F.: Case study of the effects of atmospheric aerosols and regional haze on agriculture: An opportunity to enhance crop yields in China through emission controls?, *PNAS*, 96, 13626–13633, 1999a.
- Chameides, W. L., Li, X., Tang, X., Zhou, X., Luo, C., Kiang, C. S., John, J. St., Saylor, R. D., Liu, S. C., Lam, K. S., Wang, T., and Giorgi, F.: Is ozone pollution affecting crop yields in China, *Geophys. Res. Lett.*, 26, 867–870, 1999b.
- Cooper, O. R., Parrish, D. D., Stohl, A., Trainer, M., Nedelec, P., Thouret, V., Cammas, J. P., Oltmans, S. J., Johnson, B. J., Tarasick, D., Leblanc, T., McDermid, I. S., Jaffe, D., Gao, R., Stith, J., Ryerson, T., Aikin, K., Campos, T., Weinheimer, A., and Avery, M. A.: Increasing springtime ozone mixing ratios in the free troposphere over western North America, *Nature*, 463, 344–348, doi:10.1038/nature08708, 2010.
- Dickerson, R. R., Kondragunta, S., Stenchikov, G., Civerolo, K. L., Doddridge, B. G., and Holben, B. N.: The impact of aerosols on solar ultraviolet radiation and photochemical smog, *Science*, 278, 827–830, 1997.
- Ding, A. J., Wang, T., Thouret, V., Cammas, J.-P., and Nédélec, P.: Tropospheric ozone climatology over Beijing: analysis of aircraft data from the MOZAIC program, *Atmos. Chem. Phys.*, 8, 1–13, doi:10.5194/acp-8-1-2008, 2008.
- Ding, A. J., Wang, T., Xue, L. K., Gao, J., Stohl, A., Lei, H. C., Jin, D. Z., Ren, Y., Wang, Z. F., Wei, X. L., Qi, Y. B., Liu, J., and Zhang, X. Q.: Transport of north China midlatitude cyclones: Case study of aircraft measurements in summer 2007, *J. Geophys. Res.*, 114, D08304, doi:10.1029/2008JD011023, 2009.
- Ding, A. J., Wang, T., and Fu, C. B.: Transport characteristics and origins of C transported to Hong Kong, South China, *J. Geophys. Res.*, revised, 2013a.
- Ding, A. J., Fu, C. B., Yang, X. Q., Sun, J. N., Peäjä, T., Kerminen, V.-M., Wang, T., Xie, Y. N., Herrmann, E., Zheng, L. F., Nie, W., Wei, X. L., and Kulmala, M.: Intense atmospheric pollution modifies weather: a case of mixed biomass burning with fossil fuel combustion pollution in the eastern China, *Atmos. Chem. Phys. Discuss.*, 13, 14377–14403, doi:10.5194/acpd-13-14377-2013, 2013.
- Draxler, R. R. and Hess, G. D.: An overview of the HYSPLIT 4 modeling system for trajectories dispersion and deposition, *Aust. Meteor. Mag.*, 47, 295–308, 1998.
- Eichler, H., Cheng, Y. F., Birmili, W., Nowak, A., Wiedensohler, A., Brüggemann, E., Gnauk, T., Herrmann, H., Althausen, D., Ansmann, A., Engelmann, R., Tesche, M., Wendisch, M., Zhang, Y. H., Hu, M., Liu, S., and Zeng, L. M.: Hygroscopic properties and extinction of aerosol particles at ambient relative humidity in South-Eastern China, *Atmos. Environ.*, 42, 25, 6321–6334, doi:10.1016/j.atmosenv.2008.05.007, 2008.

- Feng, Z. W., Jin, M. H., Zhang, F. Z., and Huang, Y. Z.: Effects of ground-level ozone (O_3) pollution on the yields of rice and winter wheat in the Yangtze River Delta, *J. Environ. Sci.*, 15, 3, 360–362, 2003.
- Herrmann, E., Ding, A. J., Petäjä, T., Yang, X. Q., Sun, J. N., Qi, X. M., Manninen, H., Hakala, J., Nieminen, T., Aalto, P. P., Kerminen, V.-M., Kulmala, M., and Fu, C. B.: New particle formation in the western Yangtze River Delta: first data from SORPES-station, *Atmos. Chem. Phys. Discuss.*, 13, 1455–1488, doi:10.5194/acpd-13-1455-2013, 2013.
- Kamens, R., Jang, M., Chien, C.-J., and Leach, K.: Aerosol formation from reaction of α -pinene and ozone using a gas-phase kinetics-aerosol partitioning model, *Environ. Sci. Technol.*, 33, 1430–1438, 1999.
- Khoder, M. I.: Atmospheric conversion of sulfur dioxide to particulate sulfate and nitrogen dioxide to particulate nitrate and gaseous nitric acid in an urban area, *Chemosphere*, 49, 675–684, 2002.
- Li, L., Chen, C. H., Fu, J. S., Huang, C., Streets, D. G., Huang, H. Y., Zhang, G. F., Wang, Y. J., Jang, C. J., Wang, H. L., Chen, Y. R., and Fu, J. M.: Air quality and emissions in the Yangtze River Delta, China, *Atmos. Chem. Phys.*, 11, 1621–1639, doi:10.5194/acp-11-1621-2011, 2011.
- Lin, W., Xu, X., Zhang, X., and Tang, J.: Contributions of pollutants from North China Plain to surface ozone at the Shangdianzi GAW Station, *Atmos. Chem. Phys.*, 8, 5889–5898, doi:10.5194/acp-8-5889-2008, 2008.
- Lin, W., Xu, X., Ge, B. Z., and Zhang, X. C.: Characteristics of gaseous pollutants at Gucheng, a rural site southwest of Beijing, *J. Geophys. Res.*, 114, D00G14, doi:10.1029/2008JD010339, 2009.
- Liu, H. Y., Jacob, D. J., Chan, L. Y., Oltmans, S. J., Bey, I., Yantosca, R. M., Harris, J. M., Duncan, B. N., and Martin, R. V.: Sources of tropospheric ozone along the Asian Pacific Rim: An analysis of ozonesonde observations, *J. Geophys. Res.*, 107, 4573, doi:10.1029/2001JD002005, 2002.
- Liu, P. F., Zhao, C. S., Gobel, T., Hallbauer, E., Nowak, A., Ran, L., Xu, W. Y., et al.: Hygroscopic properties of aerosol particles at high relative humidity and their diurnal variations in the North China Plain, *Atmos. Chem. Phys.*, 3479–3494, doi:10.5194/acp-11-3479-2011, 2011.
- Luo, C., St. John, J. C., Zhou, X. J., Lam, K. S., Wang, T., and Chameides, W. L.: A nonurban ozone air pollution episode over eastern China: Observation and model simulation, *J. Geophys. Res.*, 105, 1889–1908, 2000.
- Ministry of Environmental Protection of China (MEP), Ambient air quality standards (GB 3095–2012), 12 pp., China Environmental Science Press, Beijing, 2012.
- Naja, M. and Akimoto, H.: Contribution of regional pollution and long-range transport to the Asia-Pacific region: Analysis of long-term ozonesonde data over Japan, *J. Geophys. Res.*, 109, D21306, doi:10.1029/2004JD004687, 2004.
- Petäjä, T., Vakkari, V., Pohja, T., Nieminen, T., Laakso, H., Aalto P. P., Keronen, P., Siivola, E., Kerminen, V.-M., Kulmala, M., and Laakso, L.: Transportable aerosol characterization trailer with trace gas chemistry: Design, instruments and verification, *Aerosol Air Qual. Res.*, 13, 421–435, doi:10.4209/aaqr.2012.08.0207, 2013.
- Ran, L., Zhao, C. S., Xu, W. Y., Han, M., Lu, X. Q., Han, S. Q., Lin, W. L., Xu, X. B., Gao, W., Yu, Q., Geng, F. H., Ma, N., Deng, Z. Z., and Chen, J.: Ozone production in summer in the megacities of Tianjin and Shanghai, China: a comparative study, *Atmos. Chem. Phys.*, 12, 7531–7542, doi:10.5194/acp-12-7531-2012, 2012.
- Ravishankara, A. R.: Heterogeneous and multiphase chemistry in the troposphere, *Science*, 276, 1058–1065, 1997.
- Richter, A., Burrows, J. P., Nub, H., Granier, C., and Niemeier, C.: Increase in tropospheric nitrogen dioxide over China observed from space, *Nature*, 437, 129–132, doi:10.1038/nature04092, 2005.
- Stohl, A., Forster, C., Eckhardt, S., Spichtinger, N., Huntrieser, H., Heland, J., Schlager, H., Wilhelm, S., Arnold, F., and Cooper, O.: A backward modeling study of intercontinental pollution transport using aircraft measurements, *J. Geophys. Res.*, 108, 4370, doi:10.1029/2002JD002862, 2003.
- Tie, X. X. and Cao, J. J.: Aerosol pollution in China: Present and future impact on environment, *Particuology*, 7, 426–431, 2009.
- Tu, J., Xia, Z. G., Wang, H. S., and Li, W. Q.: Temporal variations in surface ozone and its precursors and meteorological effects at an urban site in China, *Atmos. Res.*, 85, 310–337, 2007.
- van Donkelaar, A., Martin, R. V., Brauer, M., Kahn, R., Levy, R., Verduzco, C., and Villeneuve, P. J.: Global estimates of ambient fine particulate matter concentrations from satellite-based aerosol optical depth: development and application, *Environ. Health Perspectives*, 118, 847–855, 2010.
- Wang, G. H., Huang, L. M., Gao, S. X., Gao, S. T., and Wang, L. S.: Characterization of watersoluble species of PM₁₀ and PM_{2.5} aerosols in urban area in Nanjing, China, *Atmos. Environ.*, 36, 1299–1307, 2002.
- Wang, G. H., Kawamura, K., Xie, M. J., Hu, S. Y., Cao, J. J., An, Z. S., Waston, J., and Chow, J. C.: Organic molecular compositions and size distributions of Chinese summer and autumn aerosols from Nanjing: Characteristic haze event caused by wheat straw burning, *Environ. Sci. Technol.*, 43, 6493–6499, 2009.
- Wang, T., Cheung, V. T. F., Anson, M., and Li, Y. S.: Ozone and related gaseous pollutants in the boundary layer of eastern China: Overview of the recent measurements at a rural site, *Geophys. Res. Lett.*, 28, 2373–2376, 2001.
- Wang, T., Ding, A. J., Blake, D. R., Zahorowski, W., Poon, C. N., and Li, Y. S.: Chemical characterization of the boundary layer outflow of air pollution to Hong Kong during February–April 2001, *J. Geophys. Res.*, 108, 8787–8801, doi:10.1029/2002JD003272, 2003.
- Wang, T., Wong, C. H., Cheung, T. F., Blake, D. R., Arimoto, R., Baumann, K., Tang, J., Ding, G. A., Yu, X. M., Li, Y. S., Streets, D. G., and Simpson, I. J.: Relationships of trace gases and aerosols and the emission characteristics at Lin'an, a rural site in eastern China, during spring 2001, *J. Geophys. Res.*, 109, D19S05, doi:10.1029/2003JD004119, 2004.
- Wang, T., Ding, A. J., Gao, J., and Wu, W. S.: Strong ozone production in urban plumes from Beijing, China, *Geophys. Res. Lett.*, 33, L21806, doi:10.1029/2006GL027689, 2006.
- Wang, T., Wei, X. L., Ding, A. J., Poon, C. N., Lam, K. S., Li, Y. S., Chan, L. Y., and Anson, M.: Increasing surface ozone concentrations in the background atmosphere of Southern China, 1994–2007, *Atmos. Chem. Phys.*, 9, 6217–6227, doi:10.5194/acp-9-6217-2009, 2009.
- Wang, T., Nie, W., Gao, J., Xue, L. K., Gao, X. M., Wang, X. F., Qiu, J., Poon, C. N., Meinardi, S., Blake, D., Wang, S. L., Ding, A. J.,

- Chai, F. H., Zhang, Q. Z., and Wang, W. X.: Air quality during the 2008 Beijing Olympics: secondary pollutants and regional impact, *Atmos. Chem. Phys.*, 10, 7603–7615, doi:10.5194/acp-10-7603-2010, 2010.
- Wang, Y., Zhuang, G. S., Zhang, X. Y., Huang, K., Xu, Chang, Tang, A. H., Chen, J. M., and An, Z. S.: The ion chemistry, seasonal cycle, and sources of PM_{2.5} and TSP aerosol in Shanghai, *Atmos. Environ.*, 40, 2935–2952, 2006.
- Wang, Y., Hao, J., McElroy, M. B., Munger, J. W., Ma, H., Chen, D., and Nielsen, C. P.: Ozone air quality during the 2008 Beijing Olympics: effectiveness of emission restrictions, *Atmos. Chem. Phys.*, 9, 5237–5251, doi:10.5194/acp-9-5237-2009, 2009.
- Xu, X., Lin, W., Wang, T., Yan, P., Tang, J., Meng, Z., and Wang, Y.: Long-term trend of surface ozone at a regional background station in eastern China 1991–2006: enhanced variability, *Atmos. Chem. Phys.*, 8, 2595–2607, doi:10.5194/acp-8-2595-2008, 2008.
- Yang, H., Yu, J. Z., Ho, S. S. H., Xu, J. H., Wu, W. S., Wan, C. H., Wang, X. D., Wang, X. R., and Wang, L. S.: The chemical composition of inorganic and carbonaceous materials in PM_{2.5} in Nanjing, China, *Atmos. Environ.*, 39, 3735–3749, 2005.
- Ye, X. N., Ma, Z., Zhang, J. C., Du, H. H., Chen, J. M., Chen, H. Yang, X., Gao, W., and Geng, F. H.: Important role of ammonia on haze formation in Shanghai, *Environ. Res. Lett.*, 6, 024019, doi:10.1088/1748-9326/6/2/024019, 2011.
- Zhang, L. M., Gong, S. L., Padro, J., and Barrie, L.: A size-segregated particle dry deposition scheme for an atmospheric aerosol module, *Atmos. Environ.*, 35, 549–560, 2001.
- Zhang, M., Chen, J. M., Chen, X. Y., Cheng, T. T., Zhang, Y. L., Zhang, H. F., Ding, A. J., Wang, M., and Melouki, A.: Urban aerosol characteristics during the World Expo 2010 in Shanghai, *Aerosol. Air Quality Res.*, 13, 36–48, doi:10.4209/aaqr.2012.02.0024, 2013.
- Zhang, Y. H., Hu, M., Zhong, L. J., Wiedensohler, A., Liu, S. C., Andreae, M. O., Wang, W., and Fan, S. J.: Regional integrated experiments on air quality over Pearl River Delta 2004 (PRIDE-PRD2004): Overview, *Atmos. Environ.*, 42, 6157–6173, 2008.
- Zhang, R. J., Xu, Y. F., and Han, Z. W.: Inorganic chemical composition and source signature of PM_{2.5} in Beijing during ACE-Asia period, *Chinese Sci. Bull.*, 48, 10, 1002–1005, 2003.
- Zhang, Q., Streets, D. G., Carmichael, G. R., He, K. B., Huo, H., Kannari, A., Klimont, Z., Park, I. S., Reddy, S., Fu, J. S., Chen, D., Duan, L., Lei, Y., Wang, L. T., and Yao, Z. L.: Asian emissions in 2006 for the NASA INTEX-B mission, *Atmos. Chem. Phys.*, 9, 5131–5153, doi:10.5194/acp-9-5131-2009, 2009.
- Zhou, X. H., Gao, J., Wang, T., Wu, W. S., and Wang, W. X.: Measurement of black carbon aerosols near two Chinese megacities and the implications for improving emission inventories, *Atmos. Environ.*, 43, 3918–3924, 2009.